Supporting Information

Probing Thermal Stability in $CsPbI_3$ Quantum Dots with Coupled Pb-Site Doping and Halide Passivation

Pouriya Naziri[1,2], Saba Sepahban Shahgoli[1,2], Hadi Jahangiri[3], Umut Aydemir[2,4]*

[1] Graduate School of Sciences and Engineering, Koç University, Istanbul-34450, Türkiye

[2] Koç University Boron and Advanced Materials Application and Research Center (KUBAM), Istanbul-34450, Türkiye

[3] Koç University Surface Science and Technology Center (KUYTAM), Istanbul-34450, Türkiye

[4] Department of Chemistry, Koç University, Istanbul-34450, Türkiye

* Corresponding author, Email: uaydemir@ku.edu.tr

Table of Contents

Section 1 Calculation of Percentage Size and Lattice-Spacing Changes............................. 3

Section 2 Biexponential PL Decay Analysis and Recombination Dynamics........................ 4

Section 3 Radiative and Non-Radiative Recombination Rates... 6

Section 4 Temperature-Dependent Optical Bandgap Extraction... 7

Section 5 FTIR Vibrational Analysis.. 8

Section S1. Calculation of Percentage Size and Lattice-Spacing Changes

To quantitatively assess the thermal microstructural evolution of $CsPbI_3$-based QDs, the percentage variations in mean particle size (Δsize) and interplanar spacing (Δd) were calculated using the following equations. The mean diameters were extracted from TEM size-distribution histograms (N ≥ 100), while d-spacings were obtained from HR-TEM lattice-fringe analyses. Smaller Δsize and Δd values correspond to enhanced lattice rigidity, reduced coalescence, and improved thermal stability of the QDs during heating.

These parameters were derived from the TEM size distributions and HR-TEM lattice-fringe measurements before and after heat treatment to assess nanoscale thermal stability.

Percentage size change (%Δsize) was calculated as

$$\%\Delta size = \frac{(Mean\ size_{AHT} - Mean\ size_{BHT})}{Mean\ size_{BHT}} \times 100$$

where "Mean size" corresponds to the average QD diameter obtained from the particle-size histograms (N ≥ 100).

Percentage change in d-spacing (%Δd) was calculated as

$$\%\Delta d = \frac{(d_{AHT} - d_{BHT})}{d_{BHT}} \times 100$$

using interplanar spacing values ($d_{(200)}$) derived from HR-TEM lattice-fringe analysis.

A smaller %Δsize and %Δd indicate enhanced structural rigidity, reduced coalescence, and superior thermal microstructural stability of the QDs under heating.

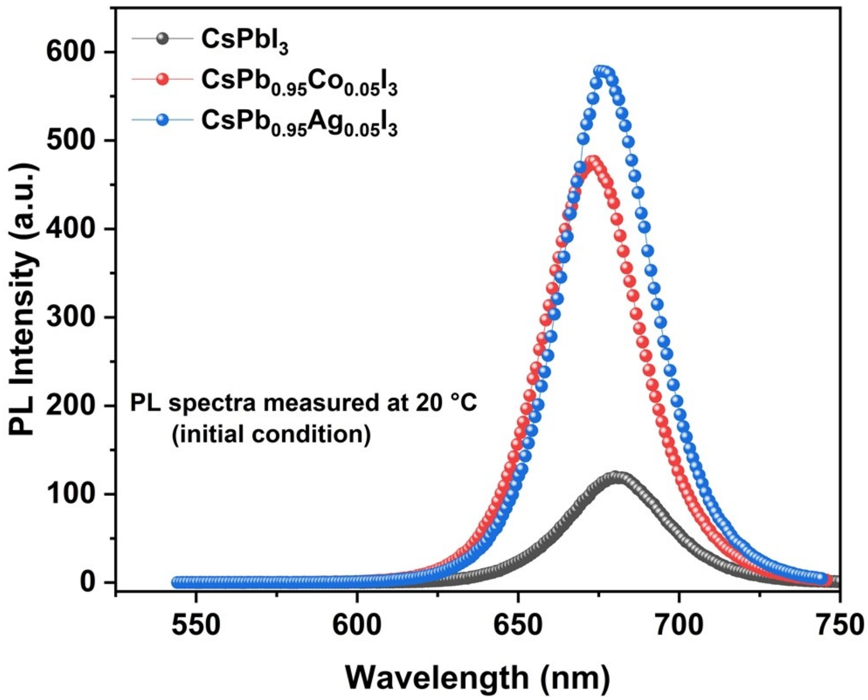

Figure S1. Photoluminescence spectra of pristine $CsPbI_3$ and $CsPb_{0.95}Co_{0.05}I_3$ and $CsPb_{0.95}Ag_{0.05}I_3$ QDs measured at 20 °C (initial condition) under identical excitation. The doped samples show significantly enhanced PL intensity and improved spectral definition relative to pristine $CsPbI_3$, indicating reduced nonradiative recombination prior to thermal aging.

Section S2. Biexponential PL decay analysis and recombination dynamics

The time-resolved PL decay curves were fitted using a biexponential decay function of the form:

$$I(t) = A_1 \cdot exp(-\frac{t}{\tau_1}) + A_2 \cdot exp(-\frac{t}{\tau_2})$$

Where,

τ_1 and τ_2 are the decay lifetimes of the fast and slow components, respectively, and A_1 and A_2 are their corresponding amplitudes (normalized spectral weights of each channel in the total PL decay).

The average lifetime $\boldsymbol{\tau_{av}}$ is calculated using the standard intensity-weighted (amplitude-weighted) model:

$$\tau_{av} = \frac{\left(A_1{\tau_1}^2 + A_2{\tau_2}^2\right)}{(A_1\tau_1 + A_2\tau_2)}$$

This definition accounts for the fact that each recombination channel contributes both a characteristic lifetime and an intensity fraction. Therefore, τ_{av} reflects the effective carrier residence time in the emissive states under the actual population distribution of the decay channels.

All fitting parameters of pristine and doped QDs are summarized in Table S1-3.

Table S1: Temperature-dependent biexponential PL decay fitting parameters for pristine $CsPbI_3$ QDs obtained from time-resolved photoluminescence measurements in the range of 20-60 °C.

Temperature (°C)	A_1	τ_1 (ns)	A_2	τ_2 (ns)	τ_{av} (ns)
20	0.2125	11.39	0.7875	49.83	**47.5**
30	0.2205	12.94	0.7795	49.54	**47.0**
40	0.2391	10.22	0.7609	46.46	**44.2**
50	0.4099	15.27	0.5991	35.53	**31.0**
60	0.3425	14.32	0.5840	31.53	**27.9**

Table S2: Temperature-dependent biexponential PL decay fitting parameters for $CsPb_{0.95}Co_{0.05}I_3$ QDs obtained from time-resolved photoluminescence measurements in the range of 20-60 °C.

Temperature (°C)	A_1	τ_1 (ns)	A_2	τ_2 (ns)	τ_{av} (ns)
20	0.3912	14.52	0.5861	33.53	**29.2**
30	0.3992	13.92	0.5961	31.53	**27.5**
40	0.2631	15.87	0.7369	28.64	**26.5**
50	0.2732	15.94	0.9465	25.05	**26.0**
60	0.3052	6.12	0.6001	22.89	**24.4**

Table S3: Temperature-dependent biexponential PL decay fitting parameters for $CsPb_{0.95}Ag_{0.05}I_3$ QDs obtained from time-resolved photoluminescence measurements in the range of 20-60 °C.

Temperature (°C)	A_1	τ_1 (ns)	A_2	τ_2 (ns)	τ_{av} (ns)
20	0.2656	15.12	0.7344	42.39	**39.3**
30	0.3804	19.24	0.6196	44.09	**38.9**
40	0.2438	12.90	0.7678	40.25	**37.7**
50	0.3096	16.13	0.6904	37.32	**33.9**
60	0.2631	11.86	0.7169	34.74	**32.2**

Section S3. Radiative and non-radiative recombination rates

The effective (average) PL lifetime can be related to the total recombination rate:

$$\tau_{av} = \frac{1}{k_r + k_{nr}}$$

Where,

k_r and k_{nr} are the radiative recombination rate and the non-radiative recombination rate constants, respectively.

This relation originates from the first-order kinetic model of carrier recombination in semiconductors and quantum dots. Upon photoexcitation, charge carriers can relax through two parallel pathways: radiative recombination, characterized by the rate constant k_r , and nonradiative recombination, characterized by k_{nr}. The total decay rate $k_r + k_{nr}$ is therefore the sum of these two independent processes. This relationship provides a qualitative understanding of how doping and temperature influence carrier recombination kinetics in the quantum dots.

To further evaluate how thermal stress activates nonradiative decay channels, the temperature evolution of τ_{av} was analyzed based on biexponential TRPL fits (Tables S1-S3). The total recombination rate is described by:

$$\frac{1}{\tau_{av}(T)} = k_r(T) + k_{nr}(T) \tag{1}$$

$$\Delta k_{nr}(T) \approx \frac{1}{\tau_{av}(T)} - \frac{1}{\tau_{av}(20^{O}C)} \tag{2}$$

In Pristine $CsPbI_3$ QDs

τ_{av} (20 °C) = 47.5 ns, τ_{av} (60 °C) = 27.9 ns

Δk_{nr} (60 °C) = 0.03584 − 0.02105 = 0.01479 ns^{-1} ≈ **1.48×10^{-2} ns^{-1}**

In $CsPb_{0.95}Co_{0.05}I_3$ QDs

τ_{av} (20 °C) = 29.2 ns, τ_{av} (60 °C) = 24.4 ns

Δk_{nr} (60 °C) = 0.04098 − 0.03425 = 0.00673 ns^{-1} ≈ **6.7×10^{-3} ns^{-1}**

In $CsPb_{0.95}Ag_{0.05}I_3$ QDs

τ_{av} (20 °C) = 39.3 ns, τ_{av} (60 °C) = 32.2 ns

Δk_{nr} (60 °C) = 0.03106 − 0.02545 = 0.00561 ns^{-1} ≈ **5.6 × 10^{-3} ns^{-1}**

Section S4. Temperature-dependent optical bandgap extraction

To quantify the optical bandgap as a function of temperature, we followed a standard direct-transition Tauc analysis. First, the absorption coefficient α(ν) was obtained from the measured absorbance A(ν) using

$$\alpha\,(\nu) = \frac{2.303\,A\,(\nu)}{d}$$

where d is the optical path length (effective film thickness or cuvette path length, depending on the measurement geometry), and the factor 2.303 converts from base-10 absorbance to natural attenuation.

For a direct bandgap semiconductor such as $CsPbI_3$-based quantum dots, the Tauc formalism assumes

$$(\alpha h\nu)^2 = A\,(h\nu - E_g)$$

where $h\nu$ is the photon energy, A is a proportionality constant, and E_g is the optical bandgap. For each temperature, $(\alpha h\nu)^2$ was plotted versus $h\nu$, and the linear region near the onset of absorption was fitted. The bandgap E_g was obtained by extrapolating this linear fit to $(\alpha h\nu)^2$=0.

The extracted temperature-dependent values are reported in Table S4 for pristine $CsPbI_3$, $CsPb_{0.95}Co_{0.05}I_3$, and $CsPb_{0.95}Ag_{0.05}I_3$ QDs.

Table S4. Optical bandgap energies (E_g) of pristine and doped $CsPbI_3$ QDs extracted from Tauc plots at different temperatures. The gradual decrease in (E_g) with increasing temperature reflects thermally induced lattice expansion and bandgap narrowing.

Temperature (°C)	$CsPbI_3$ (eV)	$CsPb_{0.95}Co_{0.05}I_3$ (eV)	$CsPb_{0.95}Ag_{0.05}I_3$ (eV)
20	1.820 ± 0.003	1.832 ± 0.003	1.820 ± 0.003
30	1.815 ± 0.004	1.823 ± 0.004	1.815 ± 0.004
40	1.794 ± 0.005	1.814 ± 0.005	1.794 ± 0.005
50	1.784 ± 0.006	1.813 ± 0.006	1.784 ± 0.006
60	1.772 ± 0.007	1.808 ± 0.006	1.772 ± 0.006
70	—	1.793 ± 0.007	1.768 ± 0.007
80	—	1.733 ± 0.003	1.765 ± 0.003

Section S5. FTIR Vibrational Analysis

Table S5. FTIR peak positions and corresponding vibrational assignments for pristine and doped $CsPbI_3$ QDs.

Wavenumber (cm^{-1})	Vibrational Assignment	Origin
2957	ν-as(C–H) asymmetric stretching	Aliphatic chain of oleic acid acid/oleylamine ligands
2924	ν-as(C–H) asymmetric stretching	Long-chain alkyl group (–CH_2–) vibrations
2857	ν-s(C–H) symmetric stretching	Alkyl group symmetric vibration
1461	δ-as(COO^-) asymmetric bending	Carboxylate group (Pb–oleate coordination)
1378	δ-s(COO^-) symmetric bending	Carboxylate vibration confirming bidentate binding
1240	ν(C–O) stretching	C–O bond in oleate anion
724	ρ(C–H) rocking	Alkyl chain terminal rocking mode

Summary of the vibrational symbols, their physical meanings, and the corresponding types of molecular motion commonly used in FTIR vibrational mode assignments (see Table S5).

Symbol	Meaning	Typical Type of Motion
ν (nu)	Stretching vibration	Bond length changes (e.g., C–H, C–O)
δ (delta)	Bending vibration (in-plane deformation)	Bond angle changes within the plane (e.g., scissoring, rocking, wagging)
ρ (rho)	Rocking vibration	In-plane rocking of CH_2 or CH_3 groups
as / s	asymmetric / symmetric	Describes whether atoms move in opposite (asymmetric) or same (symmetric) directions during vibration
γ (gamma)	Out-of-plane bending (not used in the table but sometimes appears for wagging or twisting)	